





## ARTICLE OPEN



# Emergence of Madden-Julian oscillation precipitation and wind amplitude changes in a warming climate

Hien X. Bui<sup>1</sup> , Yi-Xian Li<sup>2</sup>, Eric D. Maloney<sup>3</sup>, Ji-Eun Kim<sup>4</sup> , Sun-Seon Lee<sup>4</sup>  and Jia-Yuh Yu<sup>2</sup> 

The Madden-Julian oscillation (MJO) has profound impacts on weather and climate phenomena, and thus changes in its activity have important implications under human-induced global climate change. Here, the time at which the MJO change signal emerges from natural variability under anthropogenic warming is investigated. Using simulations of the Community Earth System Model version 2 large ensemble forced by the shared socioeconomic pathways SSP370 scenario, an increase in ensemble mean MJO precipitation amplitude and a smaller increase in MJO circulation amplitude occur by the end of the 21<sup>st</sup> century, consistent with previous studies. Notably, the MJO precipitation amplitude change signal generally emerges more than a decade earlier than that of MJO wind amplitude. MJO amplitude changes also emerge earlier over the eastern Pacific than other parts of the tropics. Our findings provide valuable information on the potential changes of MJO variability with the aim of improving predictions of the MJO and its associated extreme events.

*npj Climate and Atmospheric Science* (2023)6:22; <https://doi.org/10.1038/s41612-023-00344-z>

## INTRODUCTION

The Madden-Julian oscillation (MJO) is the dominant source of intraseasonal variability in the tropics<sup>1–4</sup> and has profound impacts on weather and climate. MJO activity can modulate tropical-extratropical interactions and extreme events in the extratropics<sup>5,6</sup>, tropical cyclone genesis<sup>7</sup>, and cooling trends in the Antarctic<sup>8</sup>, among many impacts. Previous work has shown that MJO precipitation amplitude can increase, decrease, or remain little changed in climate change simulations, depending on competing effects of an increased lower tropospheric moisture gradient and more top-heavy MJO diabatic heating profile<sup>9</sup>. In contrast, the change in MJO circulation amplitude is projected to weaken or increase at a slower rate than MJO precipitation amplitude<sup>10</sup>. Increases in MJO precipitation amplitude have been found in aquaplanet models<sup>11</sup>, single climate models<sup>12,13</sup>, multimodel analyses from the Coupled Model Intercomparison Project (CMIP) phase 3/5/6<sup>10,14,15</sup>, and also observations<sup>16</sup>. Projected increases in MJO precipitation and weakening or slower increases of MJO wind anomaly amplitude with warming are consistent with increases in dry tropical static stability, which are proportional to increases in tropical sea surface temperature (SST)<sup>17</sup>. Readers are referred to Maloney et al.<sup>18</sup> for more discussion about MJO changes under anthropogenic warming.

Although future changes in the MJO amplitude in response to global warming are likely, it remains unclear when and how these anthropogenic signals will emerge out of the background noise of natural variability. By analyzing the spread derived from a group of CMIP5 models, Bui and Maloney (2019b) noted that individual changes in multimodel mean MJO precipitation and circulation amplitude are only detectable late in the 21st century<sup>17</sup>. Before then, internal climate variability associated with decadal/interdecadal climate variations prevents the attribution of MJO change signals to greenhouse gas forcing. However, the authors also argued that decreases in the ratio of MJO wind to precipitation anomaly amplitude can be detected as early as 2021–2040,

controlled by increases in dry tropical static stability with warming. Jenney et al. (2021) added that multi-model uncertainty, which may come from the uncertainty in the parameterized moist physics in the model as mentioned by Rushley et al. (2019), also contributes to the uncertainty in future detection of the MJO characteristics<sup>19,20</sup>. In addition to the model results above, observational evidence also suggest that detecting MJO changes is complicated by interannual-to-multidecadal climate variations in the past few decades<sup>16,21</sup>.

Given the challenges in assessing MJO changes in the presence of natural variability in the climate system, we will define an index that isolates the global warming signal on the MJO from the impacts of internal climate variability. Our method is closely related to the concept of time of emergence (ToE), the time when changes in a quantity in response to anthropogenic greenhouse gas emissions deviate from natural variability<sup>22–26</sup>. Using this concept, Mora et al. (2013) showed that mean SST change signals emerge earlier in a business-as-usual scenario than a stabilization scenario, and unprecedented climates show the earliest emergence in the tropics regardless of scenario<sup>24</sup>. On interannual timescales, Ying et al. (2022) reported that changes in El Niño/Southern Oscillation (ENSO)-related rainfall variability are projected to emerge by the mid-21st century, earlier than the emergence of ENSO-related SST variability<sup>26</sup>. On weather timescales, Sippel et al. (2020) suggested that the fingerprint of climate change can be detected in the observed record of temperature since early 2012 and this detection is robust even when ignoring the long-term global warming trend<sup>25</sup>. However, on intraseasonal timescales, timing of the emergence of MJO-related change signals has received less emphasis, possibly because of complicated interactions between the MJO and other climate timescales.

Here, we will use the latest climate simulations from the Community Earth System Model version 2 large ensemble (CESM2-LE<sup>27</sup>) to (1) estimate the projected timing of when MJO change signals deviate from internal climate variability in response

<sup>1</sup>ARC Centre of Excellence for Climate Extremes, School of Earth, Atmosphere and Environment, Monash University, Clayton, Victoria, Australia. <sup>2</sup>Department of Atmospheric Sciences, National Central University, Taoyuan, Taiwan. <sup>3</sup>Department of Atmospheric Science, Colorado State University, Fort Collins, CO, USA. <sup>4</sup>Center for Climate Physics, Institute for Basic Science, Busan and Pusan National University, Busan, South Korea. ✉email: [hien.bui@monash.edu](mailto:hien.bui@monash.edu)

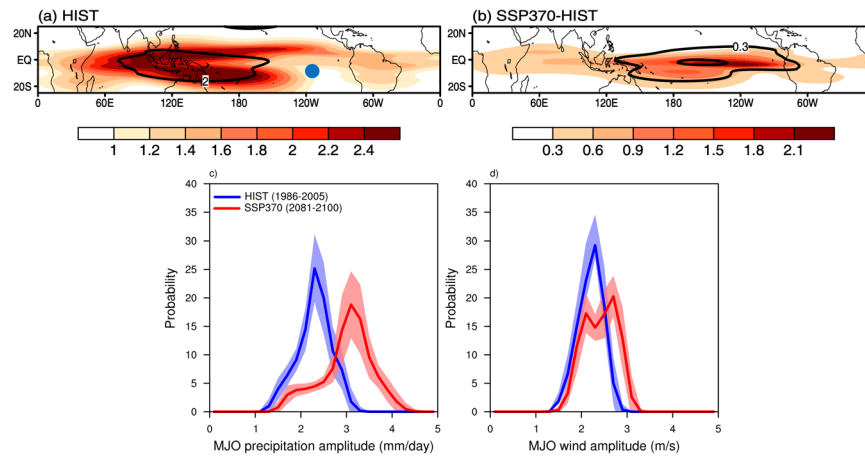


**Fig. 1 Absolute responses of MJO precipitation and wind amplitude to global warming.** **a, b** Spatial distribution of the standard deviation of 20–100 days and eastward wavenumber 1–5 filtered precipitation (shaded, units are mm/day) and 850 hPa zonal wind (contour, units are m/s) for **a** historical simulation (1986–2005) and **b** difference between SSP370 (2081–2100) and historical simulations. **c, d** Probability distribution of **c** MJO precipitation amplitude (units are mm/day) and **d** MJO wind amplitude (units are m/s) averaged over the domain of 15°S–Eq., 60°E–180° for the historical (blue) and SSP370 (red) simulations. The light blue and red shadings in **c, d** represent  $\pm 1$  standard deviation calculated across the 100 ensemble members relative to the ensemble mean. The small blue dot in **a** is the sample grid cell (5°S, 110°W) used to estimate time of emergence of MJO changes in Fig. 2.

to anthropogenic forcing and (2) examine how this projected timing of emergence varies across regions of the tropics. In addition, we will also re-assess how the MJO precipitation and wind amplitude are expected to change with global warming. The CESM2 has been documented to produce a much-improved simulation of the MJO<sup>28</sup>, especially compared to CESM1. Doing this analysis with an ensemble from a single model is preferable, as we discussed in Bui and Maloney (2019b), given a substantial internal variability in the climate system that may make conclusions drawn from single ensemble member misleading<sup>29–33</sup>. Compared to analysis with ensembles constructed from a single member from multiple models, using an ensemble from a single model avoids the differences in model architecture and parameterization<sup>27</sup>. Using a large ensemble with different initial conditions not only allows us to better characterize the entire distribution of climate variability, but also creates an improved characterization of the seasonal cycle and complex long-term trends<sup>34</sup>.

## RESULTS

### Absolute responses of MJO precipitation and wind amplitude to global warming

Before examining the time of emergence of MJO climate changes signals, we first examine the change of MJO amplitude at the end of the 21st century under global warming by comparing the historical (1986–2005) and SSP370 (2081–2100) simulations. Figure 1a shows the ensemble mean MJO-filtered precipitation and 850-hPa zonal wind standard deviation over the tropics in the historical simulation. Large MJO precipitation and zonal wind variability are found over the Indian Ocean, Maritime Continent, and western Pacific. Under global warming, the MJO precipitation amplitude increases in most regions but particularly over the Pacific and especially the East Pacific relative to historical simulation (Fig. 1b) while MJO wind amplitude shows a small increase over the central and eastern Pacific and little change over the Indo-western Pacific warm pool, consistent with previous studies using the CMIP5 models<sup>10,17</sup>. On a percentage basis, MJO precipitation amplitude changes are generally greater than wind. In addition to the change in amplitude, MJO also tends to expand further into the central and eastern Pacific, consistent with the further eastward extension of MJO activity in a warmer climate<sup>10</sup>.

Changes in MJO precipitation and wind amplitudes are further supported by an analysis of probability distributions (Fig. 1c, d). Compared to the distribution of historical period, a shift of the distribution towards a stronger amplitude of MJO precipitation and a small positive increase in wind amplitude at the end of 21st century can be seen. The shift of distribution is much larger on a percentage basis for MJO precipitation amplitude versus MJO wind amplitude, consistent with an increase in tropical dry static stability with warming<sup>17</sup>. The spread among model ensemble members (represented as standard deviation across ensemble members) is large, suggesting that natural climate variability contributes to uncertainty in determining the climate change signal of the MJO.

### Timing of MJO variability change signal under anthropogenic warming

We now examine the time of the emergence of MJO climate change signals in the tropics. Figure 2 shows an example timeseries of MJO amplitude at 5°S and 110°W (see the blue dot in Fig. 1a) from one ensemble member (i.e., cmip6.1251.002). Both MJO precipitation and wind amplitudes are relatively steady in the 20th century, with notable increases after the 2030s (c.f., Fig. 2a, b). The slope of increasing trend in MJO precipitation amplitude is larger than that in the MJO wind amplitude (i.e., 29.8% versus 6.2% change per year calculated from 2030 to 2100), supporting previous research showing that MJO wind amplitude increases at a slower rate than MJO precipitation amplitude. Based on this example, MJO precipitation amplitude (Fig. 2a) exceeds historical bounds for 3 consecutive years starting in 2027 (black arrow), 10 consecutive years starting in 2036 (blue arrow), and around 2051 (red arrow) for all subsequent years staying outside the bounds. On the other hand, MJO wind amplitude (Fig. 2b) exceeds historical bounds for all subsequent years about two decades after MJO precipitation amplitude at about 2075. Note that we estimate the year at which an individual MJO variable moves out of the historical bounds (i.e., exceed the 95th percentile of historical period) using data from the SSP370 simulation, which includes the period from 2015 to 2100 (see Methods for details). For reference, we also examine the change of dry static energy (DSE) gradient, which is proportional to change in SST (Fig. 2c), showing that a deviation from historical bounds occurs as early as the 2020s.

Considering that natural variability is different in magnitude in different regions, which generate different historical climate bounds that can be easier or more difficult to surpass for relatively small climate changes, we examine the spatial distribution of the timing of MJO amplitude change signals. Figure 3 shows the ensemble mean spatial distribution of timing for MJO precipitation and wind amplitude change signals and for different consecutive years criteria. Here, the year of emergence is first calculated for each ensemble member individually before any

ensemble averaging is done. There are several interesting points that can be derived from this analysis:

- There is a pattern mismatch between the absolute change in the MJO amplitude expected by the end of 21st century and the year at which the MJO would surpass historical precedents, especially for MJO wind (c.f., Fig. 1b and Fig. 3a–f). As previous studies mostly focused on the absolute changes of the MJO<sup>9–18</sup> (for example, MJO precipitation amplitude change from  $-10\%$  to  $+20\%$  relative to the current climate, while MJO circulation anomalies increase at a slower rate or weaken), the result here suggests that uncertainties in MJO prediction and its teleconnection impacts may be higher because both absolute changes and emergence time need to be considered.
- The projected timing of MJO precipitation amplitude changes tends to occur more than a decade earlier than MJO wind amplitude for the same consecutive year thresholds considered in regions of strongest MJO amplitude near and to the south of the equator (the time of emergence of MJO amplitude changes is also sensitive to the number of consecutive years out of historical bounds considered). An exception is over the eastern north Pacific Intertropical Convergence Zone (ITCZ) region, where MJO wind amplitude change signals tend to emerge earlier (red shaded in Fig. 3g–i). The later emergence of MJO precipitation amplitude over this region may be related to a strong anthropogenic aerosol cooling in the Northern hemisphere during 1960–1980s (i.e., interdecadal climate shift<sup>35</sup>) that further induce a stronger historical variability range in MJO precipitation. The earlier emergence of MJO precipitation amplitude change signals suggests that some aspects of climate change related to the MJO precipitation amplitude (or heating) should be expected to arrive earlier than those related to MJO circulation amplitude change.
- Unprecedented MJO activity is expected to experience the earliest occurrence over the eastern Pacific, regardless of number of consecutive years out of historical bounds (c.f., two boxes in Fig. 3). In fact, MJO precipitation amplitude over the eastern Pacific emerges about 2060s, more than a decade earlier than over the Indo-Pacific warm pool about 2080s (e.g., Fig. 3c). This is likely because of the relatively small MJO activity in the historical period in this region (c.f., Fig. 2 and

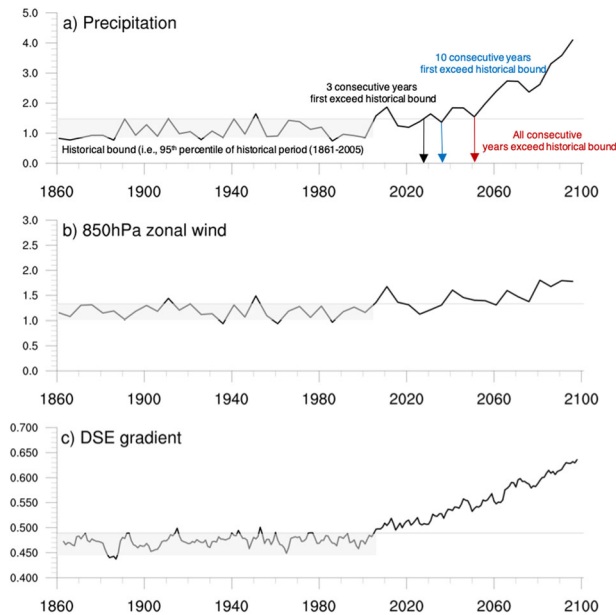


**Fig. 2** Estimating the projected timing of MJO amplitude. **a** MJO precipitation amplitude (units are mm/day), **b** 850 hPa zonal wind amplitude (units are m/s), and **c** vertical dry static energy (DSE) gradient integrated from 400–600 hPa (units are J/kg/Pa). Also indicated are the times of emergence relative to the historical bound (gray area). Fields are shown for one example member (i.e., cmip6.1251.002) at 5°S and 110°W (small blue dot in Fig. 1a). A similar plot for 5°S and 70°E is shown in Supplementary Figure 3.

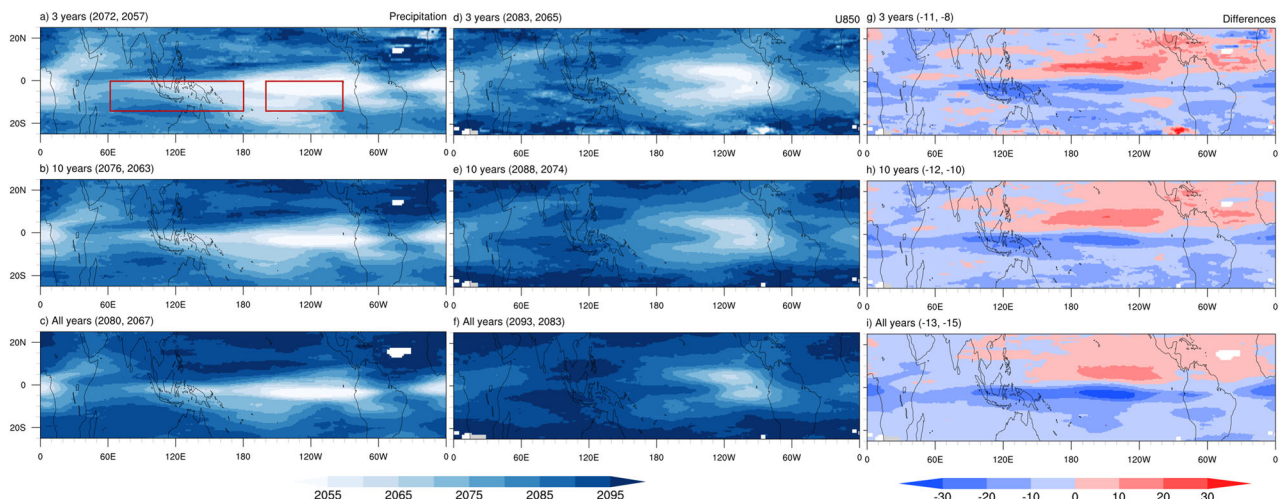


**Fig. 3** Timing of MJO variability change signal under anthropogenic warming. **a–f** Ensemble mean of the projected year when MJO precipitation and wind amplitudes exceed the historical bounds with **a, d** 3 consecutive years, **b, e** 10 consecutive years, and **c, f** all subsequent years thresholds. **g–i** Differences between the left and right panels. The number in the parentheses shows the averaged projected year over the two boxes **a** for the Indo-Pacific warm pool (15°S-Eq., 60°E-180°) and central-eastern Pacific (15°S-Eq., 90°W-160°W), respectively. See Supplementary Figure 4 for the standard deviation across ensemble members.



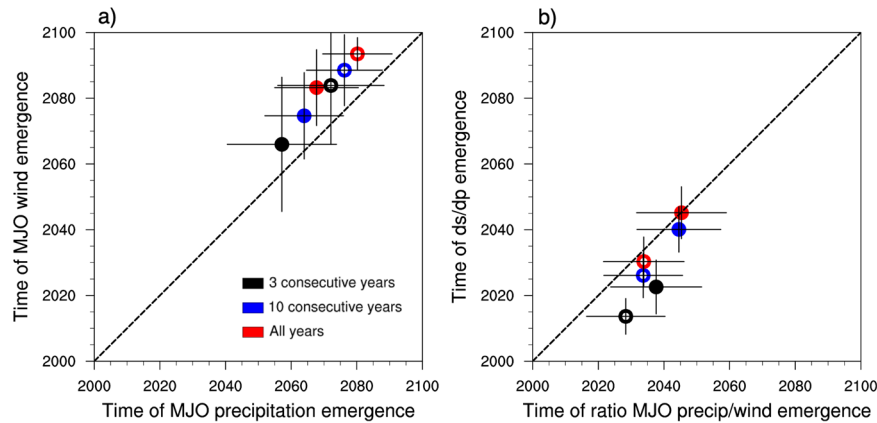


**Fig. 4 Differences in timing of emergence of MJO amplitude.** Scatterplot of the projected timing of **a** MJO precipitation amplitude (x axis) versus MJO wind amplitude (y axis) and **b** ratio between MJO precipitation to MJO wind amplitude (x axis) versus the vertical DSE gradient ( $ds/dp$ , y axis). Data are averaged over the two boxes in Fig. 3a including the Indo-Pacific warm pool (open/hollow dot,  $15^{\circ}\text{S-Eq.}, 60^{\circ}\text{E-180}^{\circ}$ ) and central-eastern Pacific (solid dot,  $15^{\circ}\text{S-Eq.}, 90^{\circ}\text{W-160}^{\circ}\text{W}$ ) for three different consecutive year thresholds to defined emergence. The bars represent the standard deviation calculated across all ensemble members from CESM2-LE. The dotted line shows a 1:1 relationship.

Supplementary Figure 3) and also the mean state changes of temperature that resembles an El Niño-like warming pattern (see also Fig. 2 in Rodgers et al., 2021). One other possibility is the southward shift of ITCZ<sup>36,37</sup> in a warmer climate, which decreases the mean precipitation in the northern tropical Pacific and is accompanied by decreases in variability. The earlier emergence of MJO amplitude change signal over the eastern Pacific may be important for impacts in the western hemisphere and teleconnections over North America<sup>38</sup>.

- To further elucidate these results, Figure. 4a shows a scatterplot of the emergence timing between MJO precipitation and MJO wind amplitude change signals averaged over the Indo-Pacific warm pool and central-eastern Pacific. Timing of emergence of MJO precipitation amplitude relative to MJO wind amplitude change signals fall along a straight line but offset from the 1:1 line, implying an earlier emergence of MJO precipitation amplitude changes compared to MJO wind amplitude changes. The earlier emergence of MJO amplitude change signals over the eastern Pacific than Indo-Pacific warm pool is also clear. The multi-model ensemble uncertainty (i.e., variability among ensemble members in the predicted year – defined as standard deviations across all ensemble members) shows a large spread (around 25 years) among ensemble members for a 3 consecutive year threshold, but a smaller spread (less than 10 years) for the 10 consecutive year and the all subsequent year thresholds (see also Supplementary Fig. 4).

Finally, to understand the differences in timing of emergence between MJO precipitation and wind amplitude change signals, we further examine the changes in mean dry static stability which is proportional to the changes in SST. On the absolute change, previous studies have shown that, a larger increase in MJO precipitation amplitude relative to MJO wind amplitude is controlled by increases in dry static stability under weak temperature gradient theory with warming<sup>18</sup>. Here, dry static stability changes emerge earlier than individual MJO precipitation and wind amplitude change signals (Fig. 2c and Fig. 4b), supporting previous arguments that dry static stability can be used to predict change in ratio of MJO precipitation and wind amplitude<sup>17</sup>. In addition, Fig. 4b shows that the timing of emergence of ratio MJO precipitation to MJO wind amplitude changes (i.e., we first calculate the ratio of MJO precipitation amplitude to MJO wind amplitude, then find the time of emergence of changes in that ratio) and the timing of dry static stability changes both occur as early as 2020–2050, and fall approximately along a 1:1 line, especially for 10-year and all

consecutive year thresholds. The result suggests that the earlier timing of emergence of MJO precipitation relative to MJO wind amplitude changes signals can be explained by earlier emergence of dry tropical static stability. The dry static stability changes over the central-eastern Pacific tend to emerge slightly later than those over the Indo-Pacific warm pool, possibly because of large ENSO variability there that creates relatively high natural variability in SST<sup>24,26</sup>.

## DISCUSSION

Understanding when the MJO at a given location will shift wholly outside the range of historical precedents with anthropogenic warming is important, given the profound impacts of MJO on extreme weather around the globe. In this study, time of emergence has been employed to isolate the impacts of internal climate variability from the global warming signal for the MJO. We have estimated the year at which MJO precipitation and wind amplitude change signals will exceed the bounds of historical climate variability (i.e., signals exceed the 95th percentile of historical periods from 1861 to 2005) using a climate change projection from the CESM2-LE under SSP370. Our primary conclusions are as follows:

- Our assessment of absolute changes in MJO amplitude in the CESM2-LE shows that MJO precipitation amplitude tends to increase with warming, while MJO wind amplitude tends to increase at a slower rate, consistent with previous studies (Fig. 1).
- The MJO precipitation amplitude change signal is detectable about a decade earlier than the MJO wind amplitude change signal, regardless of the threshold of number of consecutive years exceeding historical bounds used in the analysis (Fig. 3).
- The climate change signals of both MJO precipitation and wind amplitude tend to occur earlier over the eastern Pacific than other parts of the tropics (Fig. 3).

Since the MJO drives tropical and extratropical teleconnections through heating of the atmosphere and propagation of atmospheric waves, MJO amplitude change signals may trigger wide-ranging impacts on both the mean state and extremes events across the globe. Knowing when such MJO change signals may occur aids preparation for such changes. Our results showing an earlier emergence of MJO amplitude over the eastern Pacific (this region also has the largest precipitation amplitude change) imply increased risks of extreme events associated with MJO in this

region. Providing information on the timing of detectable MJO changes provides additional information beyond simply examining absolute changes, especially given differences in the spatial distribution between the two quantities (c.f., Fig. 1b and Fig. 3).

We admit that our estimations of time of detection of the MJO change signal depend on many factors, including the future emission scenarios used and the thresholds for the number of consecutive years out of historical bounds. However, the earlier occurrence of MJO amplitude change signals over the eastern Pacific relative to other part of the tropics is likely to be robust, especially if the pattern of SST change in the tropics looks El Niño-like. It is worth noting that while the current study focuses on the MJO, the results may imply a similar change for all daily to subseasonal timescale events. However, we note from the observed distribution of convective variance associated with various convectively coupled modes of variability that their convective variance maxima are not necessarily co-located<sup>39</sup>, and so examining implications for other convective disturbances are a topic for further research. Further, although our current methods likely remove most of the impacts of ENSO and other modes of climate variability, with the results shown mainly reflecting MJO changes, the complexity of climate system and multiscale interactions suggest that these issues require further scrutiny. Ensemble members having different initial conditions reflecting distinct timing of natural/internal variability can also generate a range of MJO change emergence times. We also note that our results may have model dependence and are worth testing with other climate models beyond CESM2. Hence, further work using ensembles from other CMIP6 models and other datasets is necessary to affirm the validity of our results and to provide more confidence in the timing of externally forced signals in MJO behaviour.

## METHODS

### Model

Here we consider 100 ensemble members from the National Center for Atmospheric Research (NCAR) CESM2-LE<sup>27</sup>. From each ensemble member, 240 years (i.e., from 1861 to 2100) of daily mean fields with a horizontal resolution of  $0.9^\circ \times 1.25^\circ$  over the historical forcing (HIST) and the shared socioeconomic pathway (SSP) with fossil-fueled development combined with a  $7 \text{ W/m}^2$  forcing scenario (SSP370<sup>40</sup>) are analyzed, where global mean surface temperature is projected to increase by about  $4.4^\circ\text{C}$  with a likely range of  $3^\circ\text{--}5^\circ$  by the end of 21st century relative to current climate. We only consider the boreal winter season (November–April) when the MJO is more active.

### Analytical methods

To examine the time of emergence of the MJO, we first create a timeseries of MJO amplitude, defined as standard deviation taken every 5 years from 1861–2100 of the 20–100 day and eastward wavenumber 1–5 filtered precipitation and 850-hPa wind at each location. This wavenumber and frequency filtering band follows the definition of the MJO domain as defined in previous studies<sup>39</sup>. While more than half of the variability in this band has been shown to be related to the MJO<sup>41</sup>, we cannot rule out that some variance associated with activity unrelated to the MJO is retained by this filter, including longer-timescale variability associated with ENSO. For example, at ENSO warm event initiation, the MJO and eastward movement of the warm pool edge associated with the growing warm event may be highly interrelated<sup>42</sup>. A filter with more narrowly confining frequency band (such as 30–80 days) produces quantitatively similar results, although the time of emergence occurs slightly later. Note that the main conclusions do not change when standard deviation is taken every 1, 10, or 20 years, although the timeseries looks noisier when standard

deviation is defined over only one year (see Supplementary Figure 1). The conclusions are also remained unchanged when using a running standard deviation rather than calculating standard deviation for discrete time chunks (Supplementary Figure 2). We then define a natural climate variability as a 95th percentile of the historical period from 1861 to 2005 for each ensemble member individually. With a larger number of years used as the historical period, a broader bound of climate variability can be archived<sup>24</sup>. Finally, we estimate the year at which an individual MJO variable moves out of the historical bounds (i.e., exceed the 95th percentile of historical period) using data from the SSP370 simulation, which includes the period from 2015 to 2100 (see Fig. 2 for details). These steps produce maps that indicate the time of emergence of a local MJO climate change signal (Fig. 3).

To define the timing of an MJO change signal emergence, we also consider the number of consecutive years out of historical bounds. As discussed by Mora et al.<sup>24</sup> the timing of a climate change signal emergence will occur sooner when fewer consecutive years out of historical bounds are considered in the definition. In fact, we will show that MJO change signals start to emerge during the 2050s when using the threshold of 3 consecutive years lying out of the historical bounds, while MJO signals tend to emerge after the 2060s when using a 10 consecutive years threshold. Admittedly, the year at which the MJO exceeds the bounds of historical variability also depends on the projection scenario. A fossil-fueled development combined with  $8.5 \text{ W/m}^2$  forcing scenario (e.g., SSP585) might produce an earlier emergence/occurrence relative to a more sustainable scenario (e.g., SSP126 or SSP245), as previously reported by Mora et al. (2013) and Ying et al.<sup>24,26</sup>. The choice of the SSP370 scenario forcing of the CESM2-LE used here follows CMIP6 recommendations<sup>40</sup> that emphasize the relatively high forcing level for the purpose of quantifying forced changes in natural variability<sup>27</sup>.

Following previous studies<sup>9,10,43</sup>, we also examine the impacts of basic state changes with warming on MJO changes. In particular, the climatological static stability defined as the monthly mean vertical average from 400 hPa to 600 hPa dry static energy (DSE) gradient  $\left(\frac{\partial s}{\partial p}\right)$ , where  $s = c_p T + gz$ , with  $T$  is temperature,  $g$  is gravity,  $z$  is the height, and  $c_p$  is specific heat of dry air at constant pressure) is analyzed to explain the timing of changes in the ratio of MJO wind to precipitation amplitude (Fig. 4).

## DATA AVAILABILITY

The CESM2-LE can be downloaded at <https://www.cesm.ucar.edu/projects/community-projects/LENS2/data-sets.html>.

## CODE AVAILABILITY

The processing codes that support the findings in this study are available from the first author upon request.

Received: 9 August 2022; Accepted: 9 March 2023;

Published online: 23 March 2023

## REFERENCES

- Madden, R. A. & Julian, P. R. Detection of a 40–50 day oscillation in the zonal wind in the tropical Pacific. *J. Atmos. Sci.* **28**, 702–708 (1971).
- Madden, R. A. & Julian, P. R. Description of global-scale circulation cells in the Tropics with a 40–50 day period. *J. Atmos. Sci.* **29**, 1109–1123 (1972).
- Zhang, C. Madden-Julian oscillation. *Rev. Geophys.* **43**, RG2003 (2005).
- Zhang, C. Madden-Julian oscillation: bridging weather and climate. *Bull. Am. Meteor. Soc.* **94**, 1849–1870 (2013).
- Cassou, C. Intraseasonal interaction between the Madden-Julian Oscillation and the North Atlantic Oscillation. *Nature* **455**, 523–527 (2008).

6. Henderson, S. A., Maloney, E. D. & Son, S.-W. Madden–Julian Oscillation Pacific teleconnections: the impact of the basic state and MJO representation in general circulation models. *J. Clim.* **30**, 4567–4587 (2017).
7. Klotzbach, P. J. The Madden–Julian Oscillation’s impacts on worldwide tropical cyclone activity. *J. Clim.* **27**, 2317–2330 (2014).
8. Hsu, P. C. et al. East Antarctic cooling induced by decadal changes in Madden-Julian oscillation during austral summer. *Sci. Adv.* **7**, eabf9903 (2021).
9. Bui, H. X. & Maloney, E. D. Mechanisms for global warming impacts on Madden-Julian Oscillation precipitation amplitude. *J. Clim.* **2**, 6961–6975 (2019).
10. Bui, H. X. & Maloney, E. D. Changes in Madden-Julian Oscillation precipitation and wind variance under global warming. *Geophys. Res. Lett.* **45**, 7148–7155 (2018).
11. Bui, H. X. & Maloney, E. D. Changes to the Madden-Julian Oscillation in coupled and uncoupled aquaplanet simulations with 4xCO<sub>2</sub>. *J. Adv. Model. Earth Syst.* **12**, e2020MS002179 (2020).
12. Adames, Á. F., Kim, D., Sobel, A. H., Del Genio, A. & Wu, J. Changes in the structure and propagation of the MJO with increasing CO<sub>2</sub>. *J. Adv. Model. Earth Syst.* **9**, 1251–1268 (2017).
13. Arnold, N. P., Branson, M., Kuang, Z., Randall, D. A. & Tziperman, E. MJO intensification with warming in the superparameterized CESM. *J. Clim.* **28**, 2706–2724 (2015).
14. Bui, H. X. & Maloney, E. D. Changes to tropical eastern north Pacific intraseasonal variability under global warming—implications for tropical cyclogenesis. *Atmósfera* **35**, 611–631 (2022).
15. Takahashi, C. et al. Projected future change of MJO and its extratropical teleconnection in East Asia during the northern winter simulated in IPCC AR4 models. *SOLA* **7**, 201–204 (2011).
16. Hsiao, W.-T., Maloney, E. D. & Barnes, E. A. Investigating recent changes in MJO precipitation and circulation in multiple reanalyses. *Geophys. Res. Lett.* **47**, e2020GL090139 (2020).
17. Bui, H. X. & Maloney, E. D. Transient response of MJO precipitation and circulation to greenhouse gas forcing. *Geophys. Res. Lett.* **46**, 13546–13555 (2019).
18. Maloney, E. D., Adames, Á. F. & Bui, H. X. Madden-Julian oscillation changes under anthropogenic warming. *Nat. Clim. Change* **9**, 26–33 (2019).
19. Jenney, A. M., Randall, D. A. & Barnes, E. A. Drivers of uncertainty in future projections of Madden–Julian Oscillation teleconnections. *Weather Clim. Dyn.* **2**, 653–673 (2021).
20. Rushley, S. S., Kim, D. & Adames, Á. F. Changes in the MJO under greenhouse gas-induced warming in CMIP5 models. *J. Clim.* **32**, 803–821 (2019).
21. Fu, Z., Hsu, P. & Liu, F. Factors regulating the multidecadal changes in MJO amplitude over the twentieth century. *J. Clim.* **33**, 9513–9529 (2020).
22. Deser, C., Knutti, R., Solomon, S. & Phillips, A. S. Communication of the role of natural variability in future North American climate. *Nat. Clim. Change* **2**, 775–779 (2012).
23. Hawkins, E. & Sutton, R. Time of emergence of climate signals. *Geophys. Res. Lett.* **39**, L01702 (2012).
24. Mora, C. et al. The projected timing of climate departure from recent variability. *Nature* **502**, 183–187 (2013).
25. Sippel, S., Meinshausen, N., Fischer, E. M., Székely, E. & Knutti, R. Climate change now detectable from any single day of weather at global scale. *Nat. Clim. Change* **10**, 35–41 (2020).
26. Ying, J. et al. Emergence of climate change in the tropical Pacific. *Nat. Clim. Change* **12**, 356–364 (2022).
27. Rodgers, K. B. et al. Ubiquity of human-induced changes in climate variability. *Earth Syst. Dyn.* **12**, 1393–1411 (2021).
28. Danabasoglu, G. et al. The community earth system model version 2 (CESM2). *J. Adv. Model. Earth Syst.* **12**, e2019MS001916 (2020).
29. Kirtman, B. Near-term climate change: Projections and predictability. In: T. F. Stocker et al. (Eds.), *Climate change 2013: The physical science basis. Contribution of Working Group I to the Fifth Assessment Report of the Intergovernmental Panel on Climate Change* (pp. 953–1028). Cambridge, United Kingdom and New York, NY, USA: Cambridge University Press (2013).
30. Pohlmann, H. et al. Predictability of the mid-latitude Atlantic meridional overturning circulation in a multi-model system. *Clim. Dyn.* **41**, 775–785 (2013).
31. Shindell, D. et al. Simultaneously mitigating near-term climate change and improving human health and food security. *Science* **335**, 183–189 (2012).
32. Teng, H. Y., Branstator, G. & Meehl, G. A. Predictability of the Atlantic overturning circulation and associated surface patterns in two CCSM3 climate change ensemble experiments. *J. Clim.* **24**, 6054–6076 (2011).
33. Wigley, T. M. L. et al. Uncertainties in climate stabilization. *Clim. Change* **97**, 85–121 (2009).
34. Haugen, M. A., Stein, M. L., Moyer, E. J. & Srivier, R. L. Estimating changes in temperature distributions in a large ensemble of climate simulations using quantile regression. *J. Clim.* **31**, 8573–8588 (2018).
35. Meehl, G. A., Hu, A. & Santer, B. D. The mid-1970s climate shift in the Pacific and the relative roles of forced versus inherent decadal variability. *J. Clim.* **22**, 780–792 (2009).
36. Rotstayn, L. D. & Lohmann, U. Tropical rainfall trends and the indirect aerosol effect. *J. Clim.* **15**, 2103–2116 (2002).
37. Hwang, Y.-T., Frierson, D. M. W. & Kang, S. M. Anthropogenic sulfate aerosol and the southward shift of tropical precipitation in the late 20th century. *Geophys. Res. Lett.* **40**, 2845–2850 (2013).
38. Zhou, W., Yang, D., Xie, S.-P. & Ma, J. Amplified Madden–Julian oscillation impacts in the Pacific–North America region. *Nat. Clim. Change* **10**, 654–660 (2020).
39. Wheeler, M. & Kiladis, G. N. Convectively coupled equatorial waves: analysis of clouds and temperature in the wavenumber–frequency domain. *J. Atmos. Sci.* **56**, 374–399 (1999).
40. O’Neill, B. C. et al. The scenario model intercomparison project (ScenarioMIP) for CMIP6. *Geosci. Model. Dev.* **9**, 3461–3482 (2016).
41. Hendon, H. H. & Wheeler, M. C. Some space–time spectral analyses of tropical convection and planetary-scale waves. *J. Atmos. Sci.* **65**, 2936–2948 (2008).
42. Levine, A. F. Z., Jin, F. F. & Stuecker, M. F. A simple approach to quantifying the noise–ENSO interaction. Part II: the role of coupling between the warm pool and equatorial zonal wind anomalies. *Clim. Dyn.* **48**, 19–37 (2017).
43. Maloney, E. D. & Xie, S.-P. Sensitivity of tropical intraseasonal variability to the pattern of climate warming. *J. Adv. Model. Earth Syst.* **5**, 32–47 (2013).

## ACKNOWLEDGEMENTS

This work was supported by Australian Research Council under grant CE170100023. E.D.M. acknowledges support from the Climate and Large-Scale Dynamics Program of the National Science Foundation under grant AGS-1841754. J.-E.K. and S.-S.L. were supported by the Institute for Basic Science project code IBS-R028-D1. We thank NCAR and IBS Center for Climate Physics (ICCP) for providing the CESM2-LE data. The authors thank Matthew Wheeler and the other anonymous reviewer for insightful comments that helped improve the manuscript.

## AUTHOR CONTRIBUTIONS

H.X.B. designed the framework of the study, performed the data analysis, and drafted the manuscript. E.D.M. contributed to discussing and interpreting the results. Y.-X.L. helped with processing codes. All authors commented on and edited the manuscript.

## COMPETING INTERESTS

The authors declare no competing interests.

## ADDITIONAL INFORMATION

**Supplementary information** The online version contains supplementary material available at <https://doi.org/10.1038/s41612-023-00344-z>.

**Correspondence** and requests for materials should be addressed to Hien X. Bui.

**Reprints and permission information** is available at <http://www.nature.com/reprints>

**Publisher’s note** Springer Nature remains neutral with regard to jurisdictional claims in published maps and institutional affiliations.



**Open Access** This article is licensed under a Creative Commons Attribution 4.0 International License, which permits use, sharing, adaptation, distribution and reproduction in any medium or format, as long as you give appropriate credit to the original author(s) and the source, provide a link to the Creative Commons license, and indicate if changes were made. The images or other third party material in this article are included in the article’s Creative Commons license, unless indicated otherwise in a credit line to the material. If material is not included in the article’s Creative Commons license and your intended use is not permitted by statutory regulation or exceeds the permitted use, you will need to obtain permission directly from the copyright holder. To view a copy of this license, visit <http://creativecommons.org/licenses/by/4.0/>.

© The Author(s) 2023